ACS OMEGA

http://pubs.acs.org/journal/acsodf

Article

# Highly Sensitive Photodetectors Based on Monolayer $MoS_2$ Field-Effect Transistors

Yuning Li, Linan Li,* Shasha Li, Jingye Sun, Yuan Fang, and Tao Deng*

Cite This: *ACS Omega* 2022, 7, 13615−13621

Read Online

ACCESS | Metrics & More | Article Recommendations

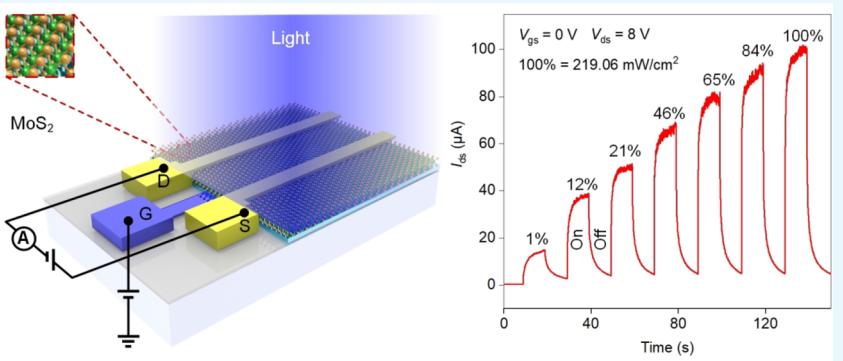


**ABSTRACT:** Molybdenum disulfide ($MoS_2$) is a promising candidate for the development of high-performance photodetectors, due to its excellent electric and optoelectronic properties. However, most of the reported $MoS_2$ phototransistors have adopted a back-gate field-effect transistor (FET) structure, requiring applied gate bias voltages as high as 70 V, which made it impossible to modulate each detecting device in the fabricated array. In this paper, buried-gate FETs based on CVD-grown monolayer $MoS_2$ were fabricated and their electric and photoelectric properties were also systematically investigated. A photoresponsivity of around 6.86 A/W was obtained at 395 nm, under the conditions of zero gate bias voltage and a light power intensity of 2.57 mW/cm$^2$. By application of a buried-gate voltage of 8 V, the photoresponsivity increased by nearly 10 times. Furthermore, the response speed of the buried-gate $MoS_2$ FET phototransistors is measured to be around 350 ms. These results pave the way for $MoS_2$ photodetectors in practical applications.

## 1. INTRODUCTION

Since the discovery of graphene, two-dimensional (2D) materials have been considered to be promising candidates for applications in next-generation optoelectronic devices due to their high carrier mobility,[1] broad coverage of their adjustable band gaps,[2] strong interaction between light and matter,[3] and high flexibility.[4,5] Among these, photodetectors based on graphene and $MoS_2$ have been intensely studied. Due to their extremely high carrier mobility, graphene photodetectors always show a high photoresponse speed.[6−8] However, graphene's zero-band-gap structure limits the photocurrent generation within the interface region between graphene and the metal electrode.[9,10] Thus, the photocurrents and photoresponsivities of graphene photodetectors are both very small. In contrast, monolayer $MoS_2$ not only has a direct band gap (1.8 eV)[11,12] but also exhibits a higher light absorption rate (11%). Furthermore, $MoS_2$ is less vulnerable to environmental changes, whose robustness to harsh vacuum and solution processes enables the tuning of its optoelectronic properties.[13] Therefore, $MoS_2$ has recently attracted more and more research attention in high-performance photodetectors.[7,14]

Since the first monolayer $MoS_2$ photodetector was demonstrated with a photoresponsivity of 7.5 mA/W and a response speed of 50 ms,[15] various $MoS_2$ photodetectors have been studied and reported. Kis et al. demonstrated a photodetector based on an exfoliated monolayer $MoS_2$ membrane, which realized an extremely high photoresponsivity of 880 A/W (at 561 nm) and a response speed (rise time) of 4 s by improvement of the mobility, contact quality, and positioning technique.[16] Through insertion of a very thin $TiO_2$ layer into the interface between the exfoliated $MoS_2$ membrane and metal electrodes to optimize the interfacial contact, Roqan

Received: December 16, 2021
Accepted: March 25, 2022
Published: April 13, 2022

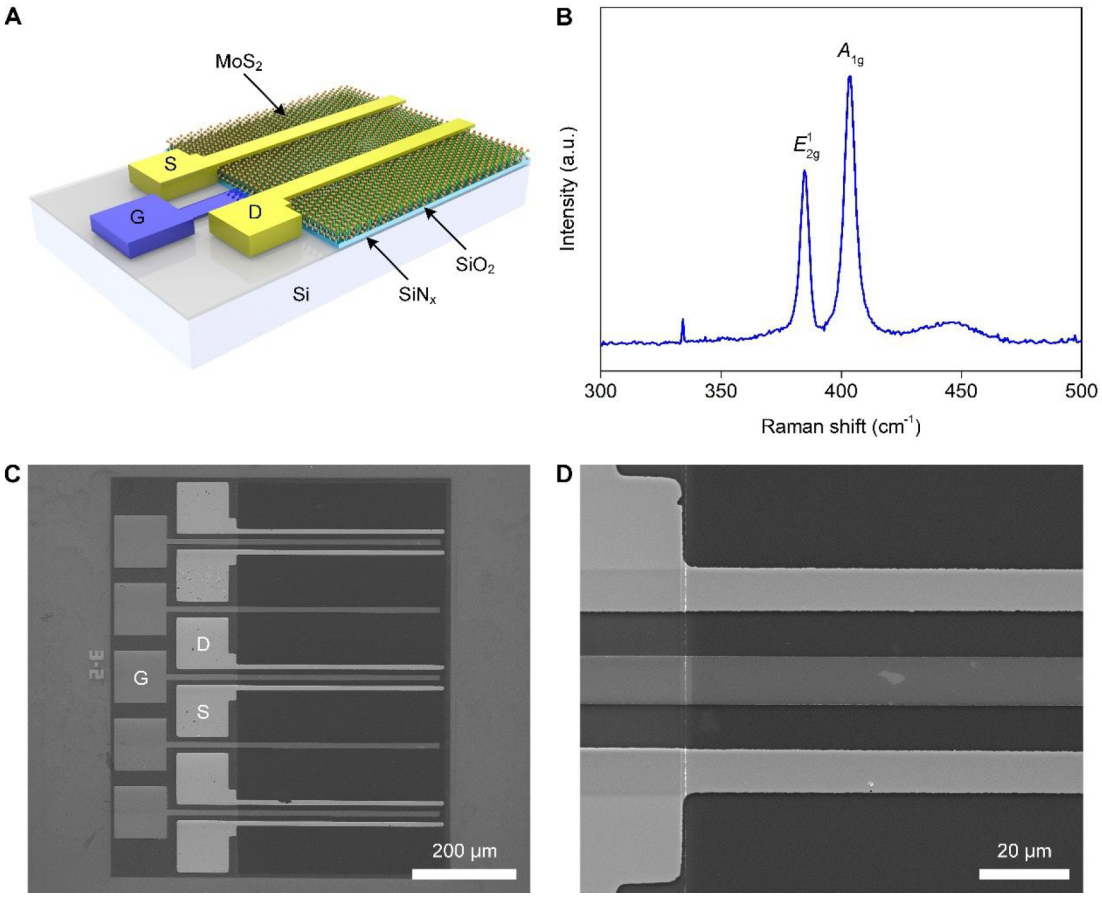


**Figure 1.** Structure characterization and Raman spectroscopy of the buried-gate $MoS_2$FETs. (A) Schematic of the buried-gate $MoS_2$ FET. (B) Raman spectrum for the conductive channel of the $MoS_2$ FET. (C) SEM image of three parallel fabricated buried-gate $MoS_2$ FETs. (D) Enlarged SEM image of the $MoS_2$ conductive channel.

et al. demonstrated a $MoS_2$ photodetector with an increase in photoresponsivity from 3 to 9 A/W (at 450 nm) and a reduction of the response speed from 5 s to less than 1 s.[13] Hu et al. improved the photoresponsivity of a monolayer $MoS_2$ photodetector from 16.9 to 377 A/W (at 360 nm) and reduced the response speed from 31 to 7.5 s by combining CVD-grown $MoS_2$ with carbon quantum dots.[17] Recently, Zhang et al. increased the photoresponsivity of few-layer $MoS_2$ photodetectors from 13.46 to 26 A/W (at 660 nm) and obtained a photoresponse speed of about several seconds, by integrating gold nanoellipse arrays on a few-layer $MoS_2$ nanosheet.[18] It is worth noting that all of the above $MoS_2$ photodetectors employed a back-gate field-effect transistor (FET) structure, which required very high gate voltages of up to 70 V.[16,19−21] The high gate voltages limit their practical applications in low-voltage and energy-saving areas. The back-gate FET structure also makes it impossible to independently modulate each device in an array, which is not conducive to applications in sensing and imaging arrays.

In this paper, monolayer $MoS_2$ FETs with a buried-gate structure were fabricated and demonstrated and their electric and photoelectric properties were systematically investigated. Under the condition of zero gate bias voltage, a photoresponsivity as high as 6.86 A/W was obtained. By application of a voltage as low as 8 V to the buried-gate electrode, the photoresponsivity can be enhanced 10 times. Furthermore, the photoresponse speed was about 350 ms. These results indicate that the buried-gate $MoS_2$ FET photodetectors have superb combination properties.

## 2. EXPERIMENTAL SECTION

The monolayer $MoS_2$ membranes were grown by the chemical vapor deposition (CVD) method, purchased from ACS Material, LLC. First, a 200 nm thick silicon nitride ($SiN_x$) passivation layer was deposited on a highly doped p-type silicon substrate. Then, a chromium (Cr)/gold (Au) electrode was sputtered on the $SiN_x$ layer, acting as the buried-gate electrode, where the thicknesses of Cr and Au layers were 10 and 30 nm, respectively. After that, a silicon dioxide ($SiO_2$) dielectric layer with a thickness of 30 nm was deposited on top of the buried-gate electrode. Next, the monolayer $MoS_2$ membrane was transferred onto the $SiO_2$ dielectric layer and patterned. Subsequently, Cr/Au (10 nm/50 nm) source and drain electrodes were evaporated on the $MoS_2$ layer, and finally, $MoS_2$ FETs with a buried-gate structure were obtained. Detailed information about the fabrication processes can be found in our previous work.[14]

The fabricated buried-gate $MoS_2$ FETs were measured using an environmental scanning electron microscope (FEI Quanta 200 ESEM FEG) operating at a beam voltage of 15 kV in high-vacuum mode. Raman spectroscopy (LabRam HR-800, Horiba Jobin Yvon) was carried out in the conductive channel of the FET to confirm the existence of $MoS_2$ and determine its layer number. The electrical properties of the devices were characterized by using a probe station (Summit 12000,


https://doi.org/10.1021/acsomega.1c07117
ACS Omega 2022, 7, 13615−13621

Cascade Microtechnology) and a semiconductor parameter analyzer (B1500A, Keysight). By integration of a light-emitting diode (LED) light-curing system (CEL-LEDS35) into the electric testing system, the photoelectrical properties of the buried-gate $MoS_2$ FETs were systematically investigated. Unless stated otherwise, all of the electric and photoelectric experiments were performed at room temperature and under ambient conditions.

## 3. RESULTS AND DISCUSSION

Figure 1A shows the schematic structure of the buried-gate $MoS_2$ FET. An SEM image of the three parallel devices

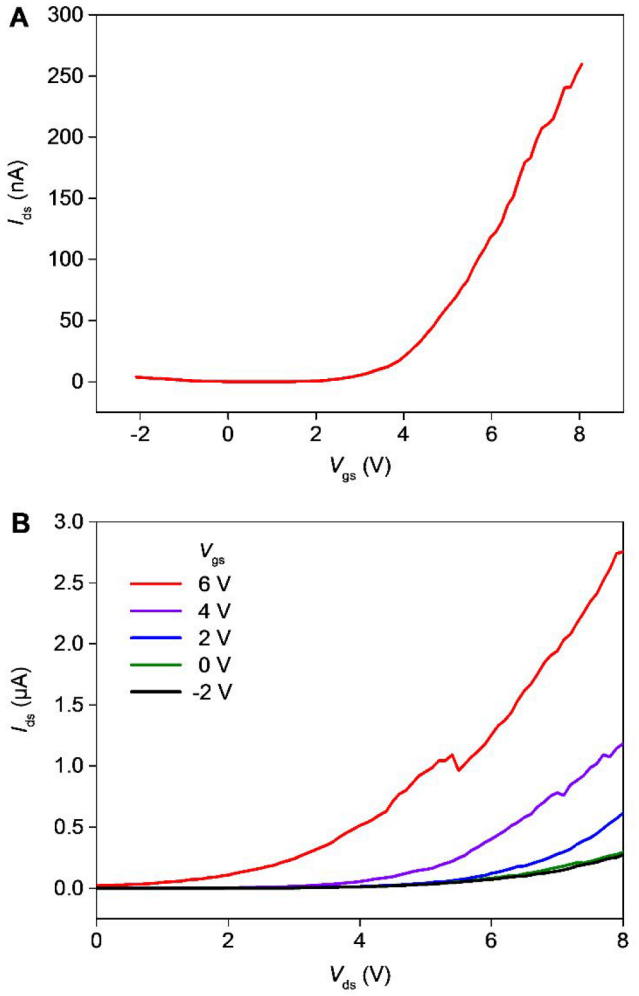


**Figure 2.** Electrical properties of the buried-gate $MoS_2$FET. (A) Transfer characteristics of the device at a source-drain voltage ($V_{ds}$) of 1 V. (B) Output characteristics of the device.

fabricated on the same $SiN_x$ passivation layer is shown in Figure 1C. The dimensions of the $MoS_2$ conductive channel are 30 $\mu$m × 400 $\mu$m, while those of the contact pad are 100 $\mu$m × 100 $\mu$m. An enlarged SEM image of one of the buried-gate $MoS_2$ FETs shown in Figure 1D demonstrates that the device was well constructed. It can be obviously seen that the gate electrode is located in the middle of the $MoS_2$ conductive channel. The widths of the source, drain, and gate electrodes are all 10 $\mu$m. In comparison with a top-gate FET structure, this structure enables the $MoS_2$ conductive channel to absorb more incident light. The existence of the $MoS_2$ membrane and

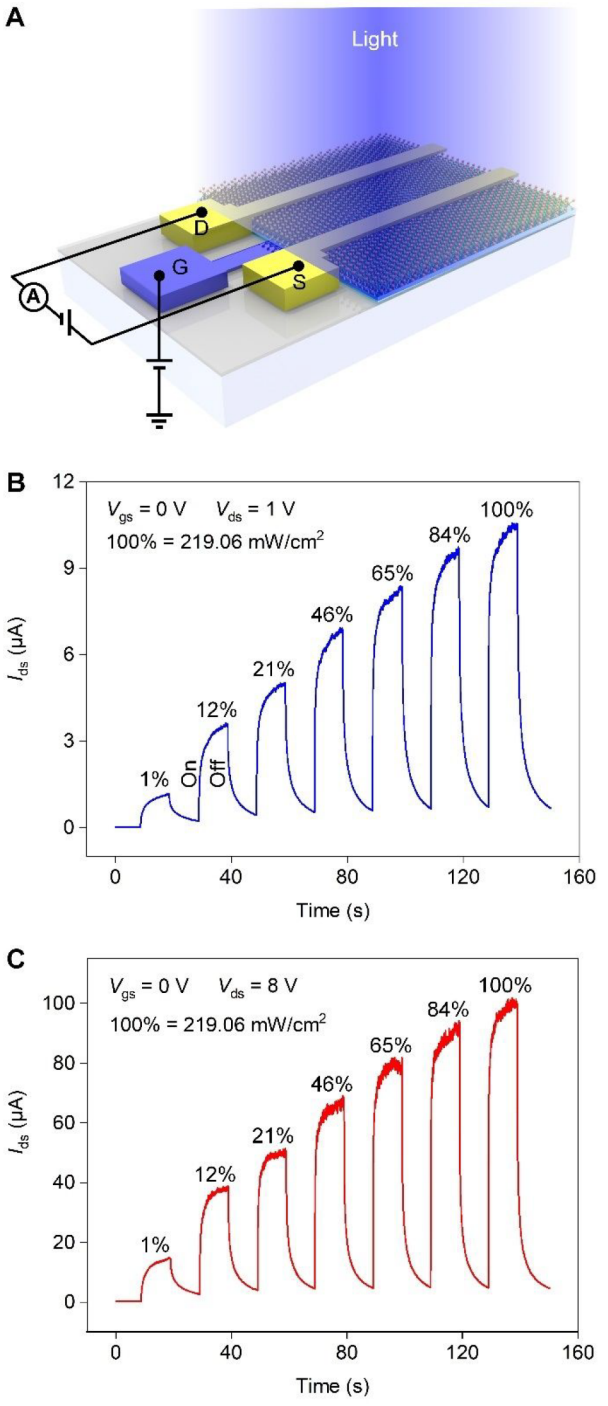


**Figure 3.** Temporal photoresponse of the buried-gate $MoS_2$ FET photodetector under the illumination of different light power densities and source-drain voltages. (A) Schematic of the experimental setup with LED illuminaiton. (B, C) Temporal photoresponses of the FET under various incident light power intensity, at source-drain voltages of 1 and 8 V, respectively. The LED light was switched on and off periodically, and the gate voltage was set to zero.

its layer number were verified and determined by Raman measurements, as shown in Figure 1B. Two peaks are seen in the figure, representing $E^1_{2g}$ and $A_{1g}$ peaks. The $E^1_{2g}$ peak is related to the in-plane vibration of two S atoms and one Mo atom inside the $MoS_2$,[22,23] which is observed at around 384.8 $cm^{-1}$. However, the $A_{1g}$ peak results from the out-of-plane



https://doi.org/10.1021/acsomega.1c07117
ACS Omega 2022, 7, 13615−13621

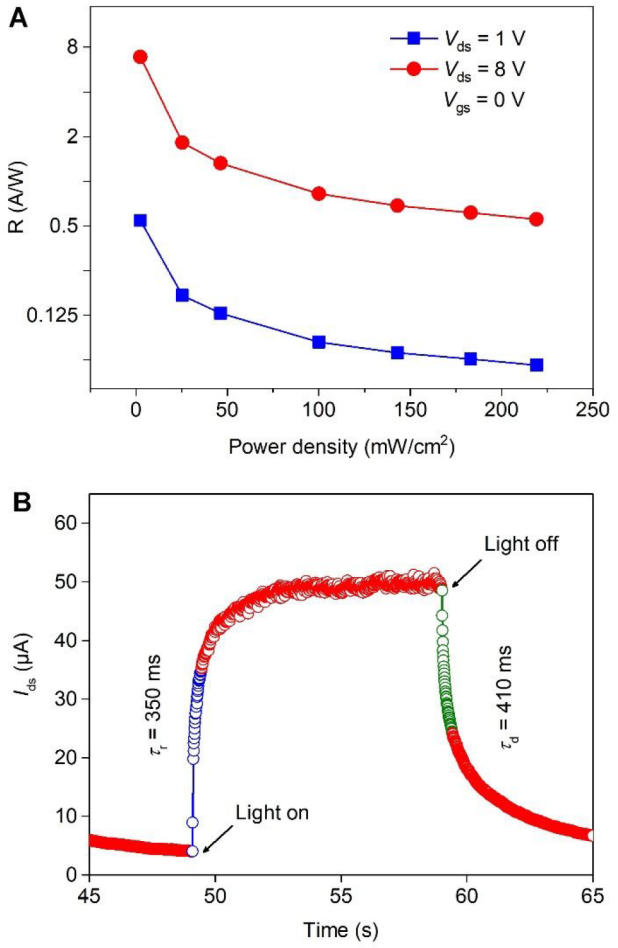


**Figure 4.** Photoresponsivity and speed of the buried-gate $MoS_2$ FET photodetector. (A) The light power intensity dependent photoresponsivity of the device under different source-drain voltages. (B) Rise ($t_r$) and decay times ($t_f$) of the photocurrent at $V_{ds}$ = 1 V and $V_{gs}$ = 0 V.

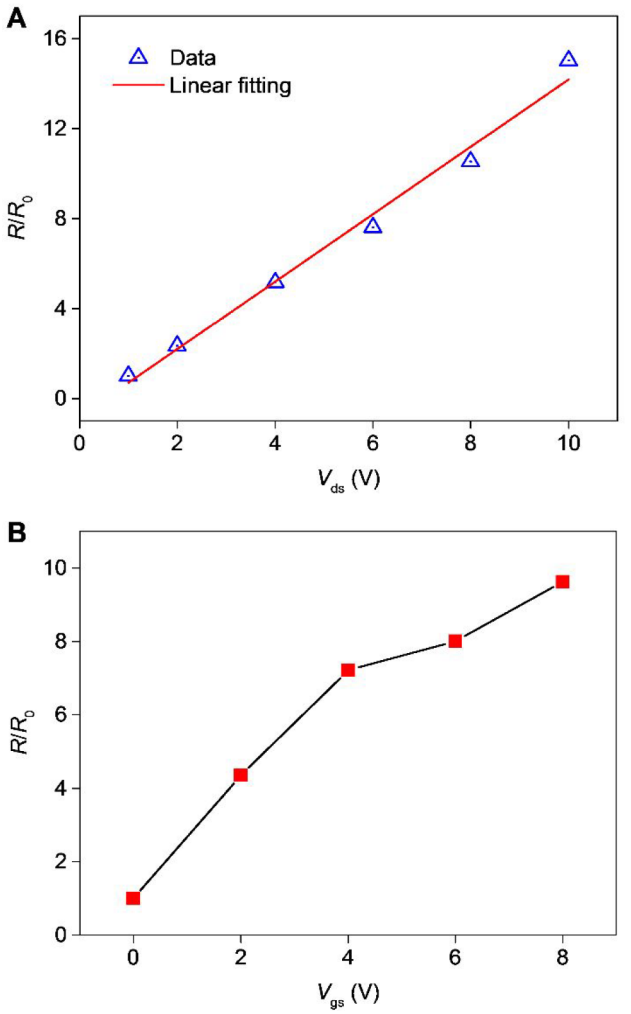


**Figure 5.** Normalized responsivities of the buried-gate $MoS_2$ FET photodetector as functions of source-drain and gate voltages. (A) Source-drain-voltage-dependent normalized photoresponsivity, where $R_0$ is the value of $R$ at $V_{gs}$ = 0 V. (B) Gate-voltage-dependent photoresponsivity at $V_{ds}$ = 1 V.

vibration of only S atoms in inverse directions,[24,25] located at about 403.8 cm$^{-1}$. The energy difference between the $E^1_{2g}$ and $A_{1g}$ Raman modes is 19 cm$^{-1}$. These results agreed well with observations of the previously reported monolayer $MoS_2$ devices[17,24−26] and verified the existence of a monolayer $MoS_2$ membrane.

Figure 2A shows the transfer characteristics of the buried-gate $MoS_2$ FET, where the source-drain current ($I_{ds}$) turns on at a gate voltage ($V_{gs}$) of 2.5 V. Hence, a typical n-type enhancement mode behavior is clearly seen. $I_{ds}$ increases significantly with an increase in $V_{gs}$ above the threshold voltage, exhibiting an on/off ratio of over $10^5$. Figure 2B shows the output characteristics of the buried-gate $MoS_2$ FET, with $V_{gs}$ varying from −2 to 6 V. When $V_{gs}$ is higher than 3 V, the current increases significantly as $V_{ds}$ increases. It is noted that $I_{ds}$ increases nonlinearly due to the unordered defective interface between the $MoS_2$ membrane and the metal electrodes. The linearity could be improved by inserting a very thin $TiO_2$ interlayer into the interface.[13] It can be seen

**Table 1. Photoelectrical Characteristics of Typical Photodetectors Based on $MoS_2$**

| description | wavelength (nm) | responsivity | detectivity (jones) | rise time (s) | ref |
|---|---|---|---|---|---|
| single-layer $MoS_2$ phototransistor | 550 | 7.5 mA/W (80 μW) | | 0.05 | 15 |
| monolayer $MoS_2$ photodetector | 561 | 880 A/W (150 pW) @ 8 V | | 4 | 16 |
| pristine $MoS_2$ photodetector | 360 | 16.9 A/W @ 5 V | $2.3 \times 10^{12}$ | 31 | 17 |
| dye-sensitized $MoS_2$ photodetector | 520 | 1.17 A/W (1 μW) @ 5 V | $1.5 \times 10^{7}$ | $5.1 \times 10^{-6}$ | 33 |
| large-scale two-dimensional $MoS_2$ photodetector | 850 | 1.8 A/W @ 5 V | $\sim 5 \times 10^{8}$ | 0.3 | 34 |
| flowerlike $MoS_2$ flexible broad-band photodetector | 405 | 0.963 A/W @ 1 V | $2.9 \times 10^{10}$ | 9.33 | 35 |
| $MoS_2$/PGS photodetector | 460 | 0.25 A/W (1.373 μW) @ 20 V | $5.6 \times 10^{8}$ | 2.19 | 36 |
| photodetector based on CVD-grown 2D $MoS_2$ | 405 | 0.2907 A/W | $10^{14.84}$ | 0.0778 | 37 |
| **this work** | 395 | 6.86 A/W @ 8 V | $0.72 \times 10^{12}$ | 0.35 | |



https://doi.org/10.1021/acsomega.1c07117
ACS Omega 2022, 7, 13615−13621

that, under a certain $V_{ds}$, $I_{ds}$ increases with an increase in $V_{gs}$, indicating a good gate-control ability.

The photoelectrical characterization of the buried-gate $MoS_2$ FET was carried out by using the experimental setup shown in Figure 3A. A LED with a wavelength of 395 nm illuminated the FET. A semiconductor parameter analyzer was used to supply the source-drain and gate bias voltages and measure the $I_{ds}$ values of the device. Figure 3B,C shows the temporal photoresponses of the FET under different incident light power densities and source-drain voltages ($V_{ds}$), where the full power density is 219.1 mW/cm$^2$. It can be seen from both graphs that, when the light is switched on, $I_{ds}$ increases immediately and significantly and gradually reaches a saturation state. When the light is switched off, $I_{ds}$ decreases promptly and markedly and then gradually returns to its original level. These behaviors were also observed in other reported back-gate $MoS_2$ FET photodetectors and could be ascribed to a photoconductive effect (or a photovoltaic effect).[24,27−29] The photocurrent ($I_{ph}$) is defined as $I_{ph} = I_{on} - I_{off}$, where $I_{on}$ and $I_{off}$ are the values of $I_{ds}$ when the light is on and off, respectively. Furthermore, it can be seen that $I_{ph}$ increases when the incident light power intensity increases from 2.57 to 219.06 mW/cm$^2$. Under the conditions of maximum incident light power intensity, zero gate bias voltage, and 1 V source-drain voltage, the value of $I_{ph}$ reached 10.56 $\mu$A (as shown in Figure 3B), which is 3500 times higher than that of a reported back-gate monolayer $MoS_2$ FET (3 nA at 580 nm, $V_{ds}$ = 1 V, $V_{gs}$ = −7 V, 0.1 mW/cm$^2$).[26] This value is also significantly higher than that in the previous work of our group (0.87 $\mu$A at 395 nm, $V_{ds}$ = 1 V, $V_{gs}$ = 0 V, 219.06 mW/cm$^2$).[31] This phenomenon may be due to the fact that the electrode could not only collect the photogenerated carriers between the channels but also collect the photogenerated carriers on the other side. Excess photoinduced carriers cause an increase in the free carrier concentration, leading to further reduced resistance of the $MoS_2$.[7] When $V_{ds}$ is increased to 8 V, $I_{ph}$ is increased to 101.86 $\mu$A (as shown in Figure 3C), which is 10 times higher than that at $V_{ds}$ = 1 V. It is also observed that $I_{on}$ fluctuates significantly as the light power intensity increases, especially when $V_{ds}$ is high.

In order to comprehensively characterize the photodetection performance of the buried-gate $MoS_2$ FET photodetectors, the photoresponsivity ($R$) and detectivity ($D^*$) are evaluated in Figure 4. The photoresponsivity is defined as $R = I_{ph}/(PS)$, where $P$ is the light power intensity and $S$ is the area of the $MoS_2$ conductive channel. Hence, $R$ decreases as the power intensity increases, as indicated in Figure 4A, due to the photogating effect, and can be ascribed to the saturated absorption under high light power.[30] Moreover, it is clearly seen that at $V_{ds}$ = 8 V the values of $R$ are significantly higher than those at $V_{ds}$ = 1 V. A photoresponsivity value as high as 6.86 A/W is obtained, under the conditions of zero gate bias voltage, $V_{ds}$ = 8 V, and $P$ = 2.57 mW/cm$^2$, which is higher than those of most of the recently reported $MoS_2$ photodetectors without integration or combination with additional light harvesters.[13,15,34] The detectivity $D^*$ is expressed as $D^* = RS^{1/2}/(2eI_{off})^{1/2}$, where $e$ is the electron charge with a value of $1.6 \times 10^{-19}$ C. From Figure 4A, the value of $D^*$ is calculated to be $0.72 \times 10^{12}$ jones, which is also superior to those of most of the $MoS_2$ photodetectors given in Table 1.

Photoresponse speed is another important feature for a photodetector. Figure 4B shows a complete on/off cycle in which the photocurrent exhibits rise/decay and reaches a steady saturation between. The rise time ($t_r$) and decay time ($t_d$) follow the definitions used in the $MoS_2$ photodetectors reported by Roqan et al.,[13] where they are defined as the times required to reach 70% and to attenuate to 50% of the peak current, respectively. The $t_r$ and $t_d$ values of the buried-gate $MoS_2$ photodetectors are 350 and 370 ms, respectively, which are relatively faster than those of recently reported $MoS_2$ photodetectors with photoresponsivities of more than 1 A/W.[13−15] What is more, a 2D alloying strategy could be used to improve the photoresponse of the $MoS_2$ device.[32] A comparison of the performance of the buried-gate $MoS_2$ photodetectors with those of other reported $MoS_2$ photodetectors is shown in Table 1. It can be seen that the comprehensive performance of our devices is rather good.

Systematic measurements demonstrated that the normalized photoresponsivity of the buried-gate $MoS_2$ photodetector increases approximately linearly with an increase in the source-drain voltage ($V_{ds}$), as shown in Figure 5A, due to an increase in the carrier drift velocity. In contrast, the carrier transit time $T_t$ (defined as $T_t = l^2/\mu V_{ds}$, where $l$ is the device length, $\mu$ is the carrier mobility, and $V_{ds}$ is the bias voltage) decreases as $V_{ds}$ increases.[15,38] The photoresponsvity can also be enhanced by applying a proper gate bias voltage ($V_{gs}$), as shown in Figure 5B. Due to the buried-gate structure, a small $V_{gs}$ value as low as 8 V can enhance the photoresponsivity by nearly 10 times at $V_{ds}$ = 1 V, in comparison to that at $V_{gs}$ = 0 V. On consideration that at $V_{gs}$ = 0 V the photoresponsvity of the buried gate $MoS_2$ photodetector could reach 6.86 A/W (Figure 4A), the maximum photoresponsivity of the device could be very high. Most of the reported $MoS_2$ photodetectors adopt a back-gate structure, which always require much higher gate voltages of more than 50 V. For example, the ultrasensitive monolayer $MoS_2$ photodetectors demonstrated by Kis et al. required a back-gate voltage of ∼70 V.[16] Therefore, the buried-gate $MoS_2$ photodetectors proposed in this paper have a promising potential for use in low-voltage and energy-saving photoelectric fields.

## 4. CONCLUSION

Sensitive buried-gate FET photodetectors based on CVD-grown monolayer $MoS_2$ were fabricated and demonstrated. A high photoresponsivity of 6.86 A/W was obtained under zero gate bias voltage, on illumination by a LED light with a wavelength of 395 nm and a power intensity of 2.57 mW/cm$^2$. The photoresponsivity could be enhanced nearly 10 times by applying an 8 V voltage to the buried-gate electrode. Furthermore, the response speed of the buried-gate $MoS_2$ FET phototransistors is about 350 ms. This study offers a simple way to obtain high-performance and low-power $MoS_2$-based photodetector arrays.

## AUTHOR INFORMATION

### Corresponding Authors

**Tao Deng** − *School of Electronic and Information Engineering, Beijing Jiaotong University, Beijing 100044, People's Republic of China*; orcid.org/0000-0001-9597-4833; Email: dengtao@bjtu.edu.cn

**Linan Li** − *School of Electronic and Information Engineering, Beijing Jiaotong University, Beijing 100044, People's Republic of China*; Email: lnli@bjtu.edu.cn



https://doi.org/10.1021/acsomega.1c07117
ACS Omega 2022, 7, 13615−13621

### Authors

**Yuning Li** − *School of Electronic and Information Engineering, Beijing Jiaotong University, Beijing 100044, People's Republic of China;* orcid.org/0000-0002-1778-8629

**Shasha Li** − *School of Electronic and Information Engineering, Beijing Jiaotong University, Beijing 100044, People's Republic of China*

**Jingye Sun** − *School of Electronic and Information Engineering, Beijing Jiaotong University, Beijing 100044, People's Republic of China*

**Yuan Fang** − *School of Electronic and Information Engineering, Beijing Jiaotong University, Beijing 100044, People's Republic of China*

Complete contact information is available at: https://pubs.acs.org/10.1021/acsomega.1c07117


### Notes

The authors declare no competing financial interest.

## ■ ACKNOWLEDGMENTS

This research was funded by the Beijing Natural Science Foundation (4202062), the National Natural Science Foundation of China (61604009), the National Science Foundation of China (Grant No. 61901028), and the 173 Key Basic Research Project (No. 2020-JCJQ-ZD-043).

## ■ REFERENCES


(1) Guo, Z.; Chen, S.; Wang, Z.; Yang, Z.; Liu, F.; Xu, Y.; Wang, J.; Yi, Y.; Zhang, H.; Liao, L.; Chu, P. K.; Yu, X. F. Metal-Ion-Modified Black Phosphorus with Enhanced Stability and Transistor Performance. *Adv. Mater.* **2017**, *29*, 1703811.

(2) Wang, F.; Wang, Z.; Yin, L.; Cheng, R.; Wang, J.; Wen, Y.; Shifa, T. A.; Wang, F.; Zhang, Y.; Zhan, X.; He, J. 2D library beyond graphene and transition metal dichalcogenides: a focus on photodetection. *Chem. Soc. Rev.* **2018**, *47* (16), 6296−6341.

(3) Britnell, L.; Ribeiro, R. M.; Eckmann, A.; Jalil, R.; Belle, B. D.; Mishchenko, A.; Kim, Y. J.; Gorbachev, R. V.; Georgiou, T.; Morozov, V.; Grigorenko, A. N.; Geim, A. K.; Casiraghi, C.; Neto, A. H. C.; Novoselov, K. S. Strong light-matter interactions in heterostructures of atomically thin films. *Science.* **2013**, *340*, 1311.

(4) Akinwande, D.; Petrone, N.; Hone, J. Two-dimensional flexible nanoelectronics. *Nat. Commun.* **2014**, *5*, 5678.

(5) Zhu, W.; Yogeesh, M. N.; Yang, S.; Aldave, S. H.; Kim, J. S.; Sonde, S.; Tao, L.; Lu, N.; Akinwande, D. Flexible black phosphorus ambipolar transistors, circuits and AM demodulator. *Nano Lett.* **2015**, *15* (3), 1883−1890.

(6) Koppens, F. H.; Mueller, T.; Avouris, P.; Ferrari, A. C.; Vitiello, M. S.; Polini, M. Photodetectors based on graphene, other two-dimensional materials and hybrid systems. *Nat. Nanotechnol.* **2014**, *9* (10), 780−793.

(7) Long, M.; Wang, P.; Fang, H.; Hu, W. Progress, Challenges, and Opportunities for 2D Material Based Photodetectors. *Adv. Funct. Mater.* **2019**, *29* (19), 1803807.

(8) Deng, T.; Zhang, Z.; Liu, Y.; Wang, Y.; Su, F.; Li, S.; Zhang, Y.; Li, H.; Chen, H.; Zhao, Z.; Li, Y.; Liu, Z. Three-Dimensional Graphene Field-Effect Transistors as High-Performance Photodetectors. *Nano Lett.* **2019**, *19* (3), 1494−1503.

(9) Zhang, B. Y.; Liu, T.; Meng, B.; Li, X.; Liang, G.; Hu, X.; Wang, Q. J. Broadband high photoresponse from pure monolayer graphene photodetector. *Nat. Commun.* **2013**, *4*, 1811.

(10) Mueller, T.; Xia, F.; Avouris, P. Graphene photodetectors for high-speed optical communications. *Nat. Photonics* **2010**, *4* (5), 297−301.

(11) Mak, K. F.; Lee, C.; Hone, J.; Shan, J.; Heinz, T. F. Atomically thin $MoS_2$: a new direct-gap semiconductor. *Phys. Rev. Lett.* **2010**, *105* (13), 136805.

(12) Mak, K. F.; He, K.; Lee, C.; Lee, G. H.; Hone, J.; Heinz, T. F.; Shan, J. Tightly bound trions in monolayer $MoS_2$. *Nat. Mater.* **2013**, *12* (3), 207−211.

(13) Pak, Y.; Park, W.; Mitra, S.; Sasikala Devi, A. A.; Loganathan, K.; Kumaresan, Y.; Kim, Y.; Cho, B.; Jung, G.-Y.; Hussain, M. M.; Roqan, I. S. Enhanced performance of $MoS_2$ photodetectors by inserting an ALD-processed $TiO_2$ interlayer. *Small* **2018**, *14* (5), 1703176.

(14) Deng, T.; Li, S.; Li, Y.; Zhang, Y.; Sun, J.; Yin, W.; Wu, W.; Zhu, M.; Wang, Y.; Liu, Z. Polarization-sensitive photodetectors based on three-dimensional molybdenum disulfide ($MoS_2$) field-effect transistors. *Nanophotonics* **2020**, *9* (16), 4719−4728.

(15) Yin, Z.; Li, H.; Li, H.; Jiang, L.; Shi, Y.; Sun, Y.; Lu, G.; Zhang, Q.; Chen, X. D.; Zhang, H. Single-layer $MoS_2$ phototransistors. *ACS Nano* **2012**, *6*, 74.

(16) Lopez-Sanchez, O.; Lembke, D.; Kayci, M.; Radenovic, A.; Kis, A. Ultrasensitive photodetectors based on monolayer $MoS_2$. *Nat. Nanotechnol.* **2013**, *8* (7), 497−501.

(17) Liu, H.; Gao, F.; Hu, Y.; Zhang, J.; Wang, L.; Feng, W.; Hou, J.; Hu, P. Enhanced photoresponse of monolayer $MoS_2$ through hybridization with carbon quantum dots as efficient photosensitizer. *2D Mater.* **2019**, *6* (3), 035025.

(18) Chen, S.; Cao, R.; Chen, X.; Wu, Q.; Zeng, Y.; Gao, S.; Guo, Z.; Zhao, J.; Zhang, M.; Zhang, H. Anisotropic plasmonic nanostructure induced polarization photoresponse for $MoS_2$-based photodetector. *Adv. Mater. Interfaces* **2020**, *7* (9), 1902179.

(19) Wang, X.; Wang, P.; Wang, J.; Hu, W.; Zhou, X.; Guo, N.; Huang, H.; Sun, S.; Shen, H.; Lin, T.; Tang, M.; Liao, L.; Jiang, A.; Sun, J.; Meng, X.; Chen, X.; Lu, W.; Chu, J. Ultrasensitive and broadband $MoS_2$ photodetector driven by ferroelectrics. *Adv. Mater.* **2015**, *27* (42), 6575−6581.

(20) Liu, X.; Yang, X.; Gao, G.; Yang, Z.; Liu, H.; Li, Q.; Lou, Z.; Shen, G.; Liao, L.; Pan, C.; Lin Wang, Z. Enhancing photoresponsivity of self-aligned $MoS_2$ field-effect transistors by piezo-phototronic effect from GaN nanowires. *ACS Nano* **2016**, *10* (8), 7451−7457.

(21) Huang, X.; Yao, Y.; Peng, S.; Zhang, D.; Shi, J.; Jin, Z. Effects of charge trapping at the $MoS_2$-$SiO_2$ interface on the stability of subthreshold swing of $MoS_2$ field effect transistors. *Materials* **2020**, *13* (13), 2896.

(22) Wang, Y.; Cong, C.; Qiu, C.; Yu, T. Raman spectroscopy study of lattice vibration and crystallographic orientation of monolayer $MoS_2$ under uniaxial strain. *Small* **2013**, *9* (17), 2857−2861.

(23) De Fazio, D.; Goykhman, I.; Yoon, D.; Bruna, M.; Eiden, A.; Milana, S.; Sassi, U.; Barbone, M.; Dumcenco, D.; Marinov, K.; Kis, A.; Ferrari, A. C. High responsivity, large-area graphene/$MoS_2$ flexible photodetectors. *ACS Nano* **2016**, *10* (9), 8252−8262.

(24) Furchi, M. M.; Polyushkin, D. K.; Pospischil, A.; Mueller, T. Mechanisms of photoconductivity in atomically thin $MoS_2$. *Nano Lett.* **2014**, *14* (11), 6165−6170.

(25) Li, H.; Zhang, Q.; Yap, C. C. R.; Tay, B. K.; Edwin, T. H. T.; Olivier, A.; Baillargeat, D. From bulk to monolayer $MoS_2$: evolution of Raman scattering. *Adv. Funct. Mater.* **2012**, *22* (7), 1385−1390.

(26) Lee, H. S.; Min, S. W.; Chang, Y. G.; Park, M. K.; Nam, T.; Kim, H.; Kim, J. H.; Ryu, S.; Im, S. $MoS_2$ nanosheet phototransistors with thickness-modulated optical energy gap. *Nano Lett.* **2012**, *12* (7), 3695−3700.

(27) Zhang, Y.; Li, H.; Wang, L.; Wang, H.; Xie, X.; Zhang, S. L.; Liu, R.; Qiu, Z. J. Photothermoelectric and photovoltaic effects both present in $MoS_2$. *Sci. Rep.* **2015**, *5*, 7938.

(28) Tsai, M. L.; Su, S. H.; Chang, J. K.; Tsai, D. S.; Chen, C. H.; Wu, C.; Li, L. J.; Chen, L. J.; He, J. H. Monolayer $MoS_2$ heterojunction solar cells. *ACS Nano* **2014**, *8*, 8317−8322.

(29) Hao, L. Z.; Gao, W.; Liu, Y. J.; Han, Z. D.; Xue, Q. Z.; Guo, W. Y.; Zhu, J.; Li, Y. R. High-performance n-$MoS_2$/i-$SiO_2$/p-Si heterojunction solar cells. *Nanoscale* **2015**, *7* (18), 8304−8308.

(30) Li, S.; Deng, T.; Zhang, Y.; Li, Y.; Yin, W.; Chen, Q.; Liu, Z. Solar-blind ultraviolet detection based on $TiO_2$ nanoparticles

decorated graphene field-effect transistors. *Nanophotonics* **2019**, *8* (5), 899−908.
(31) Li, Y. N.; Li, S. S.; Sun, J. Y.; Li, K.; Liu, Z. W.; Deng, T. Monolayer $MoS_2$ photodetectors with a buried-gate field-effect transistor structure. *Nanotechnology* **2022**, *33*, 075206.
(32) Mo, H.; Zhang, X.; Liu, Y.; Kang, P.; Nan, H.; Gu, X.; Ostrikov, K. K.; Xiao, S. Two-Dimensional Alloying Molybdenum Tin Disulfide Monolayers with Fast Photoresponse. *ACS Appl. Mater. Interfaces* **2019**, *11*, 39077−39087.
(33) Yu, S. H.; Lee, Y.; Jang, S. K.; Kang, J.; Jeon, J.; Lee, C.; Lee, J. Y.; Kim, H.; Hwang, E.; Lee, S.; Cho, J. H. Dye-sensitized $MoS_2$ photodetector with enhanced spectral Photoresponse. *ACS Nano* **2014**, *8*, 8285−8291.
(34) Ling, Z. P.; Yang, R.; Chai, J. W.; Wang, S. J.; Leong, W. S.; Tong, Y.; Lei, D.; Zhou, Q.; Gong, X.; Chi, D. Z.; Ang, K. W. Large-scale two-dimensional $MoS_2$ photodetectors by magnetron sputtering. *Opt. Express* **2015**, *23* (10), 13580−13586.
(35) Han, J.; Li, J.; Liu, W.; Li, H.; Fan, X.; Huang, K. A novel flexible broadband photodetector based on flower-like $MoS_2$ microspheres. *Opt. Commun.* **2020**, *473*, 125931.
(36) Liu, X.; Hu, S.; Lin, Z.; Li, X.; Song, L.; Yu, W.; Wang, Q.; He, W. High-Performance $MoS_2$ Photodetectors Prepared Using a Patterned Gallium Nitride Substrate. *ACS Appl. Mater. Interfaces* **2021**, *13* (13), 15820−15826.
(37) Jian, J.; Chang, H.; Dong, P.; Bai, Z.; Zuo, K. A mechanism for the variation in the photoelectric performance of a photodetector based on CVD-grown 2D $MoS_2$. *RSC Adv.* **2021**, *11* (9), 5204−5217.
(38) Tang, W.; Liu, C.; Wang, L.; Chen, X.; Luo, M.; Guo, W.; Wang, S.-W.; Lu, W. $MoS_2$ nanosheet photodetectors with ultrafast response. *Appl. Phys. Lett.* **2017**, *111* (15), 153502.



https://doi.org/10.1021/acsomega.1c07117
*ACS Omega* 2022, 7, 13615−13621